JACS
JOURNAL OF THE AMERICAN CHEMICAL SOCIETY
Article
pubs.acs.org/JACS

Non-Adiabatic Effects on Excited States of Vinylidene Observed with Slow Photoelectron Velocity-Map Imaging

Jessalyn A. DeVine,[†] Marissa L. Weichman,[†] Xueyao Zhou,[‡] Jianyi Ma,[§] Bin Jiang,*[,‡] Hua Guo,[∥] and Daniel M. Neumark*[,†,⊥]

[†]Department of Chemistry, University of California, Berkeley, California 94720, United States
[‡]Department of Chemical Physics, University of Science and Technology of China, Hefei, Anhui 230026, China
[§]Institute of Atomic and Molecular Physics, Sichuan University, Chengdu, Sichuan 610065, China
[∥]Department of Chemistry and Chemical Biology, University of New Mexico, Albuquerque, New Mexico 87131, United States
[⊥]Chemical Sciences Division, Lawrence Berkeley National Laboratory, Berkeley, California 94720, United States

Supporting Information

ABSTRACT: High-resolution slow photoelectron velocity-map imaging spectra of cryogenically cooled $\tilde{X}^2B_2$ H_2CC^- and D_2CC^- in the region of the vinylidene triplet excited states are reported. Three electronic bands are observed and, with the assistance of electronic structure calculations and quantum dynamics on ab initio-based near-equilibrium potential energy surfaces, are assigned as detachment to the $\tilde{a}$ $^3B_2$ (T_1), $\tilde{b}$ $^3A_2$ (T_2), and $\tilde{A}$ $^1A_2$ (S_1) excited states of neutral vinylidene. This work provides the first experimental observation of the $\tilde{A}$ singlet excited state of H_2CC. While regular vibrational structure is observed for the $\tilde{a}$ and $\tilde{A}$ electronic bands, a number of irregular features are resolved in the vicinity of the $\tilde{b}$ band vibrational origin. High-level ab initio calculations suggest that this anomalous structure arises from a conical intersection between the $\tilde{a}$ and $\tilde{b}$ triplet states near the $\tilde{b}$ state minimum, which strongly perturbs the vibrational levels in the two electronic states through nonadiabatic coupling. Using the adiabatic electron affinity of H_2CC previously measured to be 0.490(6) eV by Ervin and co-workers [*J. Chem. Phys.* **1989**, *91*, 5974], term energies for the excited neutral states of H_2CC are found to be $T_0(\tilde{a}\ ^3B_2) = 2.064(6)$, $T_0(\tilde{b}\ ^3A_2) = 2.738(6)$, and $T_0(\tilde{A}\ ^1A_2) = 2.991(6)$ eV.

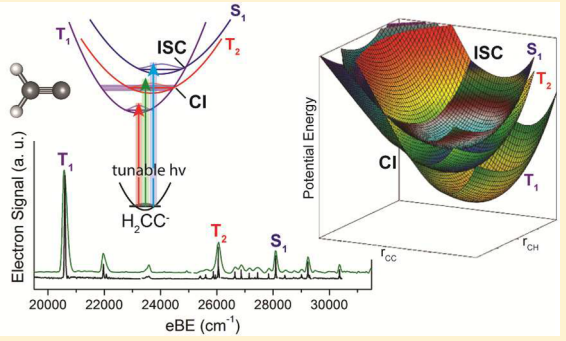

INTRODUCTION

Vinylidene (H_2CC), a high energy isomer of acetylene (HCCH) and the simplest unsaturated carbene, is an important chemical species as a reactive intermediate in a variety of processes.[1−4] Of particular importance is the vinylidene−acetylene isomerization, which serves as a prototype for 1,2-hydrogen shift reactions widely seen in organic chemistry.[5] This isomerization, believed to proceed over a remarkably low barrier (<4 kcal mol^{-1} with respect to vinylidene) barrier on the ground electronic ($\tilde{X}$) state,[6] is a benchmark unimolecular process in chemical physics and as such has been the focus of many experimental and theoretical studies.[7−14] Due to this low barrier, the spectroscopy of ground-state vinylidene is intimately connected to its possible isomerization to acetylene, and considerable effort has been devoted to detection of its spectroscopic signature among highly excited vibrational levels of HCCH.[15] Vinylidene can be probed more directly by photoelectron spectroscopy of the vinylidene anion (H_2CC^-), which has previously shown transitions to the neutral ground singlet state and low-lying triplet states with well-resolved vibrational structure.[16,17] The ground state features in these spectra were considerably broader than those of the excited states, possibly reflecting a lower barrier to isomerization in the ground state. Motivated by this earlier work, we are carrying out higher resolution experiments using slow electron velocity-map imaging of cryogenically cooled vinylidene anions (cryo-SEVI). In this paper, we report spectra for detachment to the two lowest triplet ($\tilde{a}$ $^3B_2$, $\tilde{b}$ $^3A_2$) states of vinylidene along with the first experimental observation of an excited singlet ($\tilde{A}$ $^1A_2$) state.

The first experimental evidence for the observation of vinylidene was reported in 1980, when the H_2CC species was identified as a possible carrier of a transient signal in the absorption spectrum of acetylene.[18] Vinylidene has since been proposed as a key intermediate in a number of photochemical reactions, highlighting its relevance to the study of reactive species.[19−21] Extensive studies of acetylene near the threshold of isomerization in its ground electronic state have been carried out by Field and co-workers,[22] whose results pointed to traces of vinylidene in the stimulated emission pumping spectra of acetylene and provided an estimate of ∼1.88 eV for the energy

Received: September 29, 2016
Published: November 27, 2016

DOI: 10.1021/jacs.6b10233
J. Am. Chem. Soc. 2016, 138, 16417−16425

of the H_2CC minimum relative to HCCH on the neutral $\tilde{X}$ electronic surface. Vinylidene has also been found to be a relevant isomer of dicationic acetylene; experiments probing photofragmentation following double ionization of acetylene indicate that the $HCCH^{2+}$ dication proceeds through a vinylidene configuration prior to dissociation, with an isomerization lifetime of less than 60 fs.[23,24] Given the apparent importance of the transient vinylidene species, characterization of its vibronic properties is of great interest and can provide a more complete picture of the C_2H_2 system, especially when considered in the context of the long history of experimental investigations of acetylene.[25−31]

Fortunately, the vinylidene isomer constitutes the global minimum on the anionic electronic surface of C_2H_2, providing a straightforward route to formation of neutral H_2CC by removal of an electron from the relatively stable vinylidene anion.[32−35] To date, the most quantitative data regarding excited states of vinylidene remain the vibrationally resolved anion photoelectron spectra reported by Ervin et al., who observed detachment from the H_2CC^- anion and its isotopologues to the three lowest electronic ($\tilde{X}\ ^1A_1$, $\tilde{a}\ ^3B_2$, and $\tilde{b}\ ^3A_2$) states of vinylidene.[16] Their results provided the adiabatic electron affinity (EA) of neutral vinylidene, as well as term energies of 2.065(6) and 2.75(2) eV for the two lowest triplet excited states. Several vibrational features were observed and assigned in the $\tilde{a}$ electronic band, but these spectra were limited to binding energies below ∼3.5 eV, preventing detachment to levels above the $\tilde{b}$ vibrational ground state. Peaks in the $\tilde{X}$ band were found to be broader than features arising from detachment to the excited triplet states, suggesting rapid (<200 fs) isomerization of the singlet state to an unresolved quasicontinuum of acetylene states. However, Coulomb explosion imaging experiments implied a much longer-lived vinylidene species.[34]

A great deal of theoretical work has also been carried out with the goal of elucidating the electronic structure of vinylidene and calculating its isomerization barrier in excited states. Schaefer and co-workers[36−38] have investigated low-lying triplet excited states of H_2CC, reporting energetic and structural information as well as demonstrating that the barrier for isomerization to acetylene on the $\tilde{a}$ electronic surface is ∼2 eV. An additional state, the $\tilde{A}$ singlet state, was calculated by Stanton and co-workers[39,40] to lie just above the $\tilde{a}$ and $\tilde{b}$ triplet states with a similarly high barrier, and H_2CC was found to be the global minimum on this surface. Regardless of geometry, the energetic ordering of excited electronic states of the acetylene-vinylidene system is found to be $\tilde{a} < \tilde{b} < \tilde{A}$.[41,42] Recently, the photodetachment of H_2CC^- has been investigated with a full-dimensional quantum method using highly accurate potential energy surfaces (PESs) for the anion and singlet neutral ground state,[14] which reproduced all experimentally observed features in the $\tilde{X}$ electronic band;[43] as of yet, such a theoretical treatment has not been used to investigate detachment to excited states of vinylidene.

Here, we present high-resolution photoelectron spectra of H_2CC^- and D_2CC^- obtained using slow electron velocity-map imaging (SEVI), a variation of traditional photoelectron spectroscopy that employs a tunable detachment laser and velocity-map imaging (VMI) detection scheme to obtain sub-meV resolution for low kinetic energy electrons.[44] Cryogenic cooling of the ions prior to photodetachment (cryo-SEVI) enhances resolution for molecular systems and reduces spectral congestion. The reported spectra represent the first experimental observation of the first singlet excited state of vinylidene, and partial rotational resolution is obtained for detachment to the $\tilde{b}\ ^3A_2$ and $\tilde{A}\ ^1A_2$ states. Detachment to the lowest triplet $\tilde{a}\ ^3B_2$ state is observed with higher resolution than previous spectra. Due to the limited operating range of our detachment laser at the time of measurement, the ground singlet state is not reported in this work, but efforts to acquire a high-resolution photoelectron spectrum in this region are underway both at Berkeley and in the Gibson research group at Canberra.[45]

The $\tilde{a}\ ^3B_2 \leftarrow \tilde{X}\ ^2B_2$, $\tilde{b}\ ^3A_2 \leftarrow \tilde{X}\ ^2B_2$, and $\tilde{A}\ ^1A_2 \leftarrow \tilde{X}\ ^2B_2$ electronic bands are analyzed with the assistance of high-level ab initio calculations and a full-dimensional quantum dynamics treatment analogous to that performed for photodetachment to the ground singlet state.[16] While the $\tilde{a}$ and $\tilde{A}$ electronic bands are relatively well-reproduced by theory, the $\tilde{b}$ band is visibly perturbed, with a collection of irregular features near the vibrational origin of this band. This anomalous structure is attributed to a conical intersection between the $\tilde{a}$ and $\tilde{b}$ triplet states that occurs near the $\tilde{b}$ state minimum.

MATERIALS AND METHODS

Experimental Section. The cryo-SEVI method and apparatus have been described in detail previously.[44,46] Briefly, cryogenically cooled mass-selected anions are photodetached close to threshold and the resultant photoelectrons are collected and analyzed with a velocity-map imaging (VMI) detection scheme. Relatively low extraction voltages, a tunable detachment laser, and a recently redesigned VMI lens[47] provide <2 cm^{-1} spectral resolution, with the best resolution obtained for the slowest electrons.

Vinylidene ions are made by supersonic expansion of a gas mixture containing N_2O and C_2H_4 or C_2D_4 in He through a pulsed molecular beam valve equipped with a circular filament ionizer.[48] Upon injection of electrons from the ionizer, N_2O undergoes dissociative electron attachment to form O^-, which then proceeds to react with C_2H_4 or C_2D_4 to form H_2CC^- or D_2CC^-, respectively.[49] Ions are directed through a radiofrequency (rf) hexapole ion guide and a quadrupole mass filter, then deposited into a rf linear octupole ion trap held at 5 K and filled with a precooled buffer gas mixture of 20% H_2 in He. Collisions with the buffer gas efficiently cool anions to their ground vibrational state, yielding typical internal temperatures as low as 10 K for molecular systems.[50]

After ∼40 ms in the trap, ions are extracted into an orthogonal Wiley−McLaren time-of-flight mass spectrometer.[51] The ions of interest are then focused into the interaction region of a VMI electrostatic lens[52] and photodetached with the output of an Nd:YAG-pumped tunable dye laser. The photoelectrons are projected onto a 2D detector comprising two chevron-stacked microchannel plates coupled to a phosphor screen that is photographed by a CCD camera.[53] Each image is analyzed for single electron events, and the centroid of each event is binned into a grid sufficiently fine to ensure that spectral resolution is not limited by pixel size.[54]

Radial and angular photoelectron distributions are extracted from the accumulated images using the maximum entropy velocity Legendre reconstruction method.[55] The radius of a feature in the reconstructed image is converted to electron kinetic energy (eKE) by calibration with the well-characterized detachment transitions of atomic F^-.[56] Because the best resolution is obtained for low kinetic energy electrons, a SEVI spectrum consists of multiple high-resolution scans taken ∼10−100 cm^{-1} above threshold for each peak of interest; these are then scaled to match relative peak intensities observed in an overview spectrum and spliced together, yielding a composite high-resolution spectrum. Since eKE is dependent on photon energy, spectra are plotted as functions of electron binding energy (eBE), given by eBE = $h\nu$ − eKE.

Theoretical. High-level ab initio calculations for various C_2H_2 isomers were performed at the explicitly correlated internally

DOI: 10.1021/jacs.6b10233
J. Am. Chem. Soc. 2016, 138, 16417−16425

contracted multireference configuration interaction (ic-MRCI-F12) level,[57] using reference wave functions generated from state-averaged complete active space self-consistent field (SA-CASSCF) calculations with the lowest two singlet ($\tilde{X}$, $\tilde{A}$) and two triplet ($\tilde{a}$, $\tilde{b}$) states equally weighted.[58,59] A full valence active space was used with 10 electrons in 10 active orbitals, i.e., CASSCF (10, 10), excluding the 1*s* orbitals of both carbon atoms. The correlation-consistent triple-ζ basis set optimized for the explicitly correlated approach (cc-pVTZ-F12)[60] was found to converge the vertical and adiabatic excitation energies. This computational procedure, referred to as ic-MRCI-F12/cc-pVTZ-F12 hereafter, was applied throughout the subsequent geometry optimization and construction of potential energy surfaces (PESs). All calculations were carried out using the MOLPRO electronic structure computational package.[61]

Semiglobal adiabatic PESs for the $\tilde{a}$, $\tilde{b}$, and $\tilde{A}$ states of the vinylidene isomer were constructed using the permutationally invariant polynomial neural network (PIP-NN) method.[62−64] In this method, the NN input layer consists of a number of PIPs which are conveniently obtained by symmetrizing monomials of transformed internuclear distances,[65]

$$G_l = \hat{S}\prod_{i<j}^{N} p_{ij}^{l_{ij}} \tag{1}$$

where $\hat{S}$ is the symmetrization operator, which rigorously enforces the permutation symmetry in the system, and $p_{ij} = \exp(-\lambda r_{ij})$ where r_{ij} is the internuclear distance between atoms i and j and λ is a positive length parameter typically close to 1 Å^{-1}.[66] The sum of the order l_{ij} in eq 1 represents the total degree of a monomial. In this A_2B_2 type molecule, 74 PIPs up to the fourth order were included, and the NNs were trained by the Levenberg−Marquardt algorithm with the root-mean-square error (RMSE) being used as the performance function,

$$\mathrm{RMSE} = \sqrt{\frac{1}{N}\sum_{i=1}^{N}(E_t^i - E_f^i)^2} \tag{2}$$

where E_t^i and E_f^i are the target and fitted energy of the i^{th} point, and N is the total number of points in the data set. Since the points are all chosen in the vinylidene well, the resulting PESs are not expected to be accurate elsewhere. The final PESs are the average of three best fits, with overall RMSEs of 1.45, 3.57, and 3.25 meV for the $\tilde{a}$, $\tilde{b}$, and $\tilde{A}$ states, respectively. These three PESs and the anion PES developed by Han and co-workers[43] were used for the subsequent quantum dynamical calculations of the photodetachment process. Contour plots of the resultant PESs are provided in Figure S1 of the Supporting Information (SI).

The full-dimensional quantum dynamical calculations were performed using the C+HCH (2 + 1) Radau−Jacobi coordinates,[67] denoted as (r_0, r_1, r_2, θ_1, θ_2, ϕ); r_0 is the distance between C and the center of mass of CH_2, r_1 and r_2 are two Radau radial coordinates for the HCH species, θ_1 (θ_2) is the angle between vectors r_1 (r_2) and r_0, and ϕ is the relative azimuthal angle between r_1 and r_2 in the body-fixed (BF) frame, which places the z axis along r_0. The rotationless (J = 0) Hamiltonian in this coordinate system is given (in atomic units) by the following:

$$\hat{H} = -\frac{1}{2\mu_0}\frac{\partial^2}{\partial r_0^2} + \sum_{i=1}^{2}\left(-\frac{1}{2\mu_i}\frac{\partial^2}{\partial r_i^2}\right) + \sum_{i=0}^{2}\frac{\hat{j}_i^2}{2\mu_i r_i^2} + V(r_0, r_1, r_2, \theta_1, \theta_2, \phi) \tag{3}$$

where $\mu_0 = m_C(m_C + 2m_H)/(2m_C + 2m_H)$, $\mu_1 = \mu_2 = m_H$, $\hat{j}_1$ ($\hat{j}_2$) is the angular momentum operator for r_1 (r_2), and $\hat{j}_0^2 = (\hat{j}_1 + \hat{j}_2)^2$. V is the potential energy function defined in terms of the Radau−Jacobi coordinates. The Hamiltonian was discretized using a mixed grid-basis representation;[68] radial coordinates were represented with the potential optimized discrete variable representation (POVDR),[69,70] while the angular coordinates were represented by basis functions. For the D_2CC calculations, the H atoms were substituted by its heavier isotope.

The initial wave packet (Ψ_i) on a neutral PES was assumed, within the Condon approximation, to arise from a vertical transition from an eigenstate on the anion PES. The anion wave functions for the four lowest-lying rotationless vibrational levels were obtained by diagonalizing the same Hamiltonian in eq 3 substituted by the anion PES using the Lanczos method.[71] The wave packet on the neutral state PES was propagated using the real Chebyshev propagator:[72]

$$\Psi_k = 2D\hat{H}_s\Psi_{k-1} - D^2\Psi_{k-2},\ k \geq 2 \tag{4}$$

with $\Psi_1 = D\hat{H}_s\Psi_0$ and $\Psi_0 = \Psi_i$. The Hamiltonian in eq 4 was scaled to the spectral range of (−1,1) by $\hat{H}_s = (\hat{H} - H^+)/H^-$. The spectral medium, $H^+ = (H_{max} + H_{min})/2$, and half width, $H^- = (H_{max} - H_{min})/2$, were determined by the spectral extrema. Dynamical parameters used are listed in Table S1.

Photoelectron spectra were obtained from the discrete cosine Fourier transform of the Chebyshev autocorrelation functions.[73] The eigenfunctions are assigned based on the nodal structure of the wave functions. However, it should be noted that, in the severe state mixing limit, the nodal structure of the eigenfunctions is not straightforward to interpret.

RESULTS

Experimental Section. Figure 1 shows the excited state region of the vinylidene photoelectron spectrum, the focus of the present work. In this and the following figures, the green traces are low-resolution overview spectra taken with high photon energies, and the black traces represent the high-resolution SEVI scans taken closer to threshold and scaled to match the relative intensities in the overview spectra. Two regions of structure are observed, the first spanning eBE ≈ 20 000−24 000 cm^{-1} and the second more congested region above eBE = 25 000 cm^{-1}. The lower-eBE region, shown in more detail in Figure 2, exhibits regular vibrational structure in agreement with the previously reported $\tilde{a}$ band of the vinylidene anion photoelectron spectrum.[16]

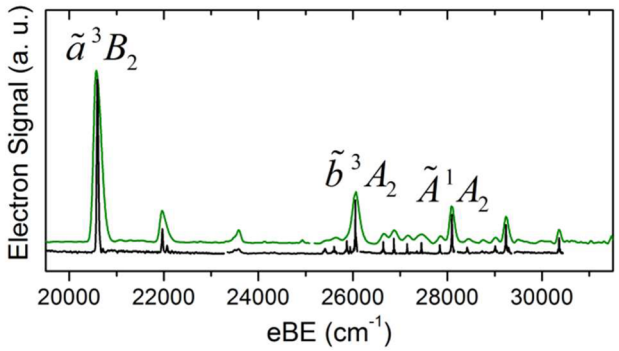

Figure 1. Anion photoelectron spectra showing detachment to the three lowest excited states of neutral H_2CC. The vibrational origin of each electronic band is labeled with the corresponding neutral state assignment. The green traces are overview spectra taken high above threshold, and the black traces correspond to composite higher-resolution, lower-eKE scans.

The higher binding energy region, shown in Figure 3 for both H_2CC^- and D_2CC^-, displays an intense peak (b1) at ∼26 000 cm^{-1} consistent with the reported binding energy of the $\tilde{b}$ band origin,[16] and, starting around 28 000 cm^{-1}, three roughly evenly spaced features (A1−A3). The 25 000−28 000 cm^{-1} region of the spectrum displays a collection of relatively weak and irregularly spaced features (labeled x), some of which appear lower in binding energy than b1. We have previously shown that vibrational cooling is very efficient under the

DOI: 10.1021/jacs.6b10233
J. Am. Chem. Soc. 2016, 138, 16417−16425

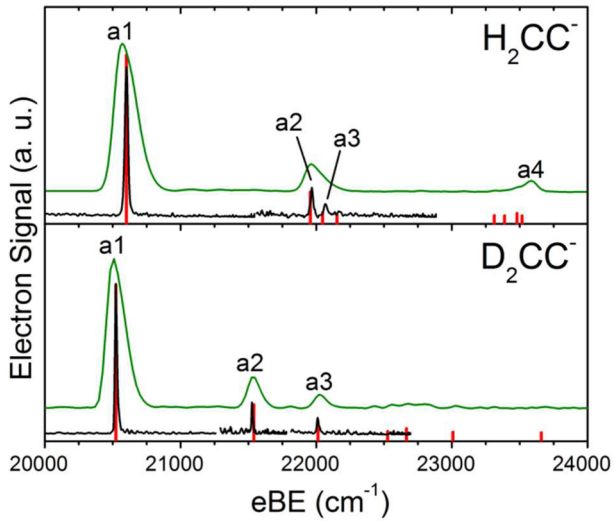

Figure 2. Cryo-SEVI spectra of H_2CC^- (top) and D_2CC^- (bottom) showing detachment to the $\tilde{a}\ ^3B_2$ state of neutral vinylidene. Green traces are low-resolution overview scans taken with high detachment energies, and the black traces are composite high-resolution scans taken closer to threshold and scaled to match the overviews. The red stick spectra show quantum dynamics results for the $\tilde{a}\ ^3B_2 \leftarrow \tilde{X}\ ^2B_2$ detachment transition.

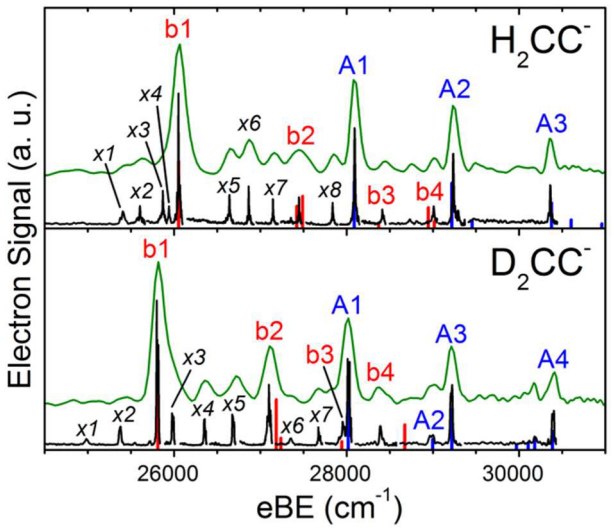

Figure 3. Cryo-SEVI spectra of H_2CC^- (top) and D_2CC^- (bottom) for the higher-eBE region of the vinylidene excited state spectrum. The green traces are low-resolution overview spectra, and the black traces are the high-resolution SEVI scans taken close to threshold and scaled to match the overviews. The stick spectra show the results of quantum dynamics for photodetachment to the $\tilde{b}\ ^3A_2$ (red) and $\tilde{A}\ ^1A_2$ (blue) states of vinylidene.

conditions used in the ion trap,[74] so these transitions are unlikely to correspond to vibrational hot bands and can be attributed to photodetachment from the ground vibrational state of the anion. This assignment is supported by the observation that the relative intensities of these features were insensitive to variations in the trap conditions. The irregular peaks are observed to shift upon deuteration, whereas the A1−A2−A3 progression does not shift substantially.

The resolution provided by cryo-SEVI is sufficient to partially resolve rotational contours for features in this region of the spectrum; representative profiles can be seen in Figure 4 for the band origins (b1 and A1) assigned in Figure 3. Rotational envelopes of other assigned features are shown in Figures S2 and S3.

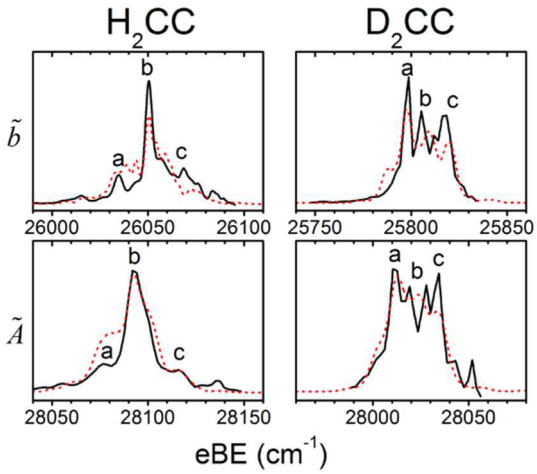

Figure 4. Rotational profiles of the $\tilde{b}$ (top) and $\tilde{A}$ (bottom) band origins in the cryo-SEVI spectra of H_2CC^- (left) and D_2CC^- (right). Experimental lineshapes are shown as solid black lines, and calculated contours are shown as red dashed lines.

In addition to detachment energies, SEVI yields the photoelectron angular distribution (PAD) associated with detachment to each neutral electronic state. For detachment with a single linearly polarized photon, the PAD is given by the following:[75]

$$\frac{d\sigma}{d\Omega} = \frac{\sigma_{tot}}{4\pi}[1 + \beta P_2(\cos\theta)] \quad (5)$$

where σ_{tot} is the total detachment cross section, $P_2(x)$ is the second-order Legendre polynomial, θ is the angle of the outgoing electron's velocity vector with respect to the laser polarization axis, and β is the anisotropy parameter. The anisotropy parameter ranges from −1 to +2 corresponding to perpendicular and parallel detachment, respectively, and contains information regarding the shape of the anion orbital from which an electron is detached.

Consideration of the anisotropies of the different features in Figure 1 reveals two distinct trends for the spectral regions shown in Figures 2 and 3. All peaks in Figure 2 have positive β values close to +2, and determination of the anisotropy parameter for the $\tilde{a}$ band vibrational origin across spectra with varying photon energies shows this to be true regardless of kinetic energy for eKE < 0.5 eV. This behavior is typical of detachment from *s*-like orbitals to form *p*-wave electrons with angular momentum $l = 1$. All features with eBE > 25 000 cm^{-1} show the same energy dependence of β, with $\beta \approx 0$ for low kinetic energies and $\beta < 0$ at moderate eKE, characteristic of detachment from *p*-like orbitals resulting in outgoing *s*- and *d*-wave electrons with $l = 0$ and 2, respectively.

According to the Wigner threshold law,[76] the cross section for photodetachment scales as $(eKE)^{l+1/2}$; as we obtain our best resolution by detaching as close to threshold as possible, the SEVI method works best for detachment transitions that can produce outgoing s-wave electrons. As such, the resolution of the $\tilde{a}$ band in Figure 2 is more limited than the $\tilde{b}$ and $\tilde{A}$ bands in Figure 3, and some of the weaker features present in the theoretical spectrum are below the detection limit for this

DOI: 10.1021/jacs.6b10233
J. Am. Chem. Soc. 2016, 138, 16417−16425

experiment. Regardless, the resolution of the $\tilde{a}$ band is somewhat improved relative to the work of Ervin and co-workers; most peaks in this region are narrower than 20 cm^{-1}, which proves sufficient to resolve the C—C stretch fundamental (a3) that was assigned, but obscured by the nearby a2 feature, in the previous study.

Electronic Structure. Figure 5 shows the ab initio energetics of various stationary states of the HCCH-H_2CC

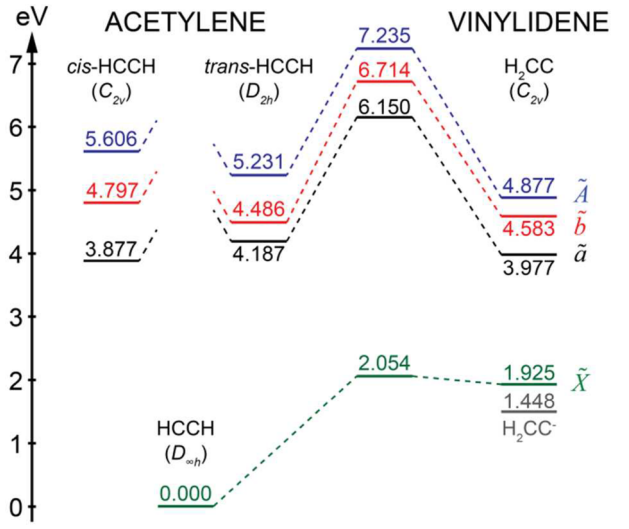

Figure 5. Energy level diagram for stationary states of the $\tilde{X}$ (gray), $\tilde{a}$ (black), $\tilde{b}$ (red), and $\tilde{A}$ (blue) states of the acetylene–vinylidene system, along with the vinylidene anion (gray), which is taken from literature for comparison.[43] Other relative energies (in eV) were obtained at the ic-MRCI-F12/cc-pVTZ-F12 level in this work.

system on the $\tilde{X}$, $\tilde{a}$, $\tilde{b}$, and $\tilde{A}$ electronic surfaces; more detailed structural information can be obtained from Figure S4 and Tables S2 and S3. As in previous works, the energy ordering of the excited states is $\tilde{a} < \tilde{b} < \tilde{A}$ regardless of geometry, and barriers for isomerization to *trans*-acetylene in excited states are large with typical values around 2 eV. In the first triplet state, *cis*-HCCH is found to be the most stable isomer, followed by vinylidene and *trans*-HCCH, though energy differences between these isomers are relatively small. In the $\tilde{b}$ state, *trans*-HCCH is slightly lower in energy than vinylidene and *cis*-HCCH, again with relatively small (~0.2 eV) energy differences between the isomers. In the singlet $\tilde{A}$ state, vinylidene becomes the global minimum, lying 0.35 and 0.73 eV lower than *trans*- and *cis*-HCCH, respectively. The equilibrium geometries of H_2CC in the $\tilde{b}$ and $\tilde{A}$ states are quite similar, with a somewhat elongated C—C bond relative to that of the $\tilde{X}$, $\tilde{a}$, and anion states. These results are in agreement with recent theoretical predictions.[38,39,41]

As a nonlinear tetratomic molecule with C_{2v} symmetry, vinylidene has six vibrational modes: the symmetric C—H stretch (ν_1, a_1), the C—C stretch (ν_2, a_1), the CH_2 scissor mode (ν_3, a_1), the out-of-plane wag (ν_4, b_1), the antisymmetric C—H stretch (ν_5, b_2), and the CH_2 rocking mode (ν_6, b_2). Harmonic frequencies for the stationary states considered in this work and their corresponding zero-point energies (ZPEs) are listed in Table S4. In the $\tilde{X}$ and $\tilde{a}$ states of vinylidene, ν_2 is higher in frequency than ν_3, whereas $\nu_2 < \nu_3$ in the $\tilde{b}$ and $\tilde{A}$ states; this is presumably due to the longer and therefore weaker C—C bond in the $\tilde{b}$ and $\tilde{A}$ states of vinylidene. It is also interesting to note that ν_1 and ν_2 are strongly mixed in the $\tilde{a}$ state due to a 1:2 Fermi resonance. In the $\tilde{b}$ state, ν_1 is strongly mixed with both ν_2 and ν_3, suggesting that there is Fermi coupling of the $1\nu_1$ state with the $2\nu_2$ and $2\nu_3$ levels. The ZPEs of H_2CC in both singlet states are similar to that of the vinylidene anion, and lower than those of the two triplet states. With ZPE corrections, the adiabatic excitation energies for $\tilde{a}$, $\tilde{b}$, and $\tilde{A}$ H_2CC are 2.091, 2.701, and 2.955 eV, respectively. The equilibrium geometries, energetics, and harmonic frequencies on all three PESs are in excellent agreement with ab initio values, demonstrating the high quality of the PIP-NN fits.

DISCUSSION

Vibronic Assignments. The calculated spectra for photodetachment of H_2CC^- and D_2CC^- are shown as red and blue sticks superimposed on the experimental spectra in Figures 2 and 3, and serve as a starting point for assignment of vibrational features. It should be noted that absolute peak positions in the calculated spectra depend sensitively on the energy difference between the anion and each neutral state, which is difficult to determine precisely at this level of theory. Indeed, the current calculation at the ic-MRCI-F12/cc-pVTZ-F12 level either overestimates by ~30 meV ($\tilde{a}$) or underestimates by ~40 meV ($\tilde{b}$ and $\tilde{A}$) the measured adiabatic excitation energies. As such, to facilitate comparison with experiment, we have artificially shifted the calculated band origin of each state to the corresponding experimental one, and focus our analysis on the relative peak positions for detachment to different vibrational levels.

Figure 2 shows that experimental peak positions and intensities for the $\tilde{a}\ ^3B_2 \leftarrow \tilde{X}\ ^2B_2$ electronic band are reproduced quite well by quantum dynamics calculations on the ab initio PES. The excellent agreement provides assignment of all resolved features. Peak positions and assignments for these features are presented in Table 1, along with the calculated

Table 1. Peak Positions (cm^{-1}), Shifts from the Origin and the Theoretical Predictions (cm^{-1}), and Assignments of Features in the $\tilde{a}\ ^3B_2 \leftarrow \tilde{X}\ ^2B_2$ Electronic Band of the Vinylidene Photoelectron Spectra[a]

peak	eBE	shift	theo.	assn.
		H_2CC		
a1	20 602 (12)	0	0	0_0^0
a2	21 968 (10)	1366	1358	3_0^1
a3	22 069 (12)	1467	1439	$2_0^1/4_0^2$
a4	23 553 (70)	2951	2921	1_0^1
		D_2CC		
a1	20 525 (8)	0	0	0_0^0
a2	21 528 (5)	1003	1002	3_0^1
a3	22 016 (9)	1491	1474	2_0^1

[a]The 2_0^1 and 4_0^2 features form a strong Fermi resonance pair for peak a3 of H_2CC. Uncertainties in peak positions correspond to one standard deviation of a Gaussian fit to the experimental peak.

frequencies. As discussed earlier, the improved resolution for this electronic band over previous work permits resolution of the close-lying a2 and a3 peaks that correspond to the ν_3 fundamental and a Fermi resonance between the $1\nu_2$ and $2\nu_4$ levels, respectively.

In Figure 3, peak b1 is assigned to the vibrational origin of the $\tilde{b}\ ^3A_2 \leftarrow \tilde{X}\ ^2B_2$ electronic band following the assignment of Ervin and co-workers.[16] Several other experimental peaks (b2-b4) roughly line up with the $\tilde{b}$ band quantum dynamics results,

DOI: 10.1021/jacs.6b10233
J. Am. Chem. Soc. 2016, 138, 16417–16425

although most of the smaller experimental peaks in Figure 3 between 25 000−28 000 cm^{-1} do not appear in the calculation. The origin of this discrepancy will be revisited below. At slightly higher eBE, comparison of the $\tilde{A}\ ^1A_2 \leftarrow \tilde{X}\ ^2B_2$ calculated spectra (blue sticks) to experiment identifies peaks A1−A3 as arising from detachment to the $\tilde{A}$ singlet state, providing an explanation for the seemingly odd trend of the spectra in Figure 3 becoming more regular at higher binding energies. This electronic assignment is supported by the identical PADs observed for all features in Figure 3, as both the $\tilde{b}$ and $\tilde{A}$ states are formed by removal of an electron from the same b_1 anion orbital.

The quantum dynamics results allow assignment of peaks b1−b4 as well as the $\tilde{A}$ band; these are reported in Tables 2 and 3 for H_2CC and D_2CC, respectively, along with experimental and theoretical peak positions. The most Franck Condon (FC) active vibrational mode in both the $\tilde{b}$ and $\tilde{A}$ electronic states is ν_2, presumably a consequence of the ∼0.1 Å increase in the C—C bond length (r_{CC}) that occurs upon photodetachment to these neutral states. The assigned progressions in this mode all present some degree of anharmonicity; consideration of the A1−A2−A3 and A1−A3−A4 progressions in Tables 2 and 3 yields harmonic frequencies of 1158(10) and 1213(10) cm^{-1} with anharmonicity constants of 8(4) and 9(4) cm^{-1} for H_2CC and D_2CC, respectively. While the 2_0^2 transition in the $\tilde{b}$ band of H_2CC^- is obscured by the ν_1 fundamental, preventing calculation of an anharmonicity constant, similar values are found for the b1−b2−b4 progression in the D_2CC^- spectrum.

Table 2. Peak Positions (cm^{-1}), Shifts from the Origin and the Theoretical Predictions (cm^{-1}), and Assignments of Features in the $\tilde{b}\ ^3A_2 \leftarrow \tilde{X}\ ^2B_2$ and $\tilde{A}\ ^1A_2 \leftarrow \tilde{X}\ ^2B_2$ Electronic Bands in the Cryo-SEVI Spectrum of H_2CC^-[a]

peak	eBE	shift	theo.	assn.
		$\tilde{b}\ ^3A_2 \leftarrow \tilde{X}\ ^2B_2$		
b1	26 035 (2)	0	0	0_0^0
b2	27 438	1403	1425	2_0^1
b3	28 400	2365	2316	4_0^2
b4	28 994	2958	2964	1_0^1
		$\tilde{A}\ ^1A_2 \leftarrow \tilde{X}\ ^2B_2$		
A1	28 077 (3)	0	0	0_0^0
A2	29 219	1142	1136	2_0^1
A3	30 345	2267	2287	2_0^2

[a]Uncertainties in peak positions, which are identical for all features in a given electronic band, correspond to one standard devation of the Gaussian convolution used to calculate the rotational contour of the band origin.

Table 3. Peak Positions (cm^{-1}), Shifts from the Origin and the Theoretical Predictions (cm^{-1}), and Assignments of Features in the $\tilde{b}\ ^3A_2 \leftarrow \tilde{X}\ ^2B_2$ and $\tilde{A}\ ^1A_2 \leftarrow \tilde{X}\ ^2B_2$ Electronic Bands in the Cryo-SEVI Spectrum of D_2CC^-[a]

peak	eBE	shift	theo.	assn.
		$\tilde{b}\ ^3A_2 \leftarrow \tilde{X}\ ^2B_2$		
b1	25 797 (2)	0	0	0_0^0
b2	27 097	1301	1370	2_0^1
b3	27 954	2157	2129	1_0^1
b4	28 387	2590	2861	2_0^2
		$\tilde{A}\ ^1A_2 \leftarrow \tilde{X}\ ^2B_2$		
A1	28 012 (3)	0	0	0_0^0
A2	28 983	971	980	3_0^1
A3	29 207	1195	1203	2_0^1
A4	30 383	2371	2375	2_0^2

[a]Uncertainties in peak positions, which are identical for all features in a given electronic band, correspond to one standard devation of the Gaussian convolution used to calculate the rotational contour of the band origin.

The experimental binding energies of peaks a1, b1, and A1, along with the electron affinity of vinylidene,[16] yield term energies of $T_0(\tilde{a}\ ^3B_2) = 2.064(6)$, $T_0(\tilde{b}\ ^3A_2) = 2.738(6)$, and $T_0(\tilde{A}\ ^1A_2) = 2.991(6)$ eV relative to the vibrational ground state of $\tilde{X}\ ^1A_1$ H_2CC, in good agreement with the ab initio results reported in this work. The term energy for the $\tilde{A}\ ^1A_2$ singlet state can be combined with the upper-bound for the energy of $\tilde{X}\ ^1A_1$ H_2CC relative to HCCH ($\Delta E \approx 1.88$ eV)[22] to place $\tilde{A}\ ^1A_2$ H_2CC at ∼4.38 eV above the ground state of acetylene. As the adiabatic excitation energy of $\tilde{A}\ ^1A_u$ *trans*-HCCH is known to be 5.219 eV,[31] our data thus confirm the predictions of Stanton and co-workers[14] that the global minimum on the first excited singlet surface of the acetylene−vinylidene system takes the vinylidene geometry.

Rotational Assignments. The resolution of the cryo-SEVI vinylidene spectra is sufficient to obtain partially resolved rotational envelopes for the vibrational origins of the $\tilde{b}$ and $\tilde{A}$ bands, as shown in Figure 4. Vinylidene is a near-prolate asymmetric top, with rotational constants $A > B \sim C$; the rotational energies for such a molecule can be approximated in terms of the quantum numbers J and K by the following:[77]

$$E_{rot}(J, K) = \frac{1}{2}(B + C)J(J + 1) + \left[A - \frac{1}{2}(B + C)\right]K^2 \quad (6)$$

Rotational constants for the ground state of vinylidene have been calculated previously from ab initio calculations.[78] For H_2CC, $A \approx 10$ cm^{-1}, whereas B and C are on the order of 1 cm^{-1}, so the resolution provided by SEVI is only sufficient to assign rotational branches corresponding to changes in K.

As was shown in our previous consideration of the partially resolved rotational profiles in the SEVI spectra of CH_2CN^- and CD_2CN^-,[79] the selection rule for photodetachment requires that $\Delta K = K_{neutral} - K_{anion} = \pm 1$. Allowed values of K_{anion} for H_2CC^- (D_2CC^-), considering both ortho and para nuclear spin states, are governed by the requirement that the total internal wave function be antisymmetric (symmetric) with respect to hydrogen interchange.[80] In the $\tilde{X}\ ^2B_2$ anion state, we find that *o*-H_2CC^- and *p*-D_2CC^- are restricted to even values of K_{anion}, whereas *p*-H_2CC^- and *o*-D_2CC^- must have odd K_{anion}. Given the low internal temperatures typical of the cryo-SEVI experiment, we expect most of our anions to be in the $K = 0$ (*o*-H_2CC^-, *p*-D_2CC^-) or $K = 1$ (*p*-H_2CC^-, *o*-D_2CC^-) states, so the rotational contour will consist primarily of three branches, corresponding to the $1 \leftarrow 0$ and $0, 2 \leftarrow 1$ rotational transitions. The relative intensities of these branches are dictated by nuclear spin statistics directly analogous to those of H_2 (D_2); applied to H_2CC^- (D_2CC^-), this results in a 3:1 (1:2) ratio of the $K = 0$:$K = 1$ anion population. These considerations allow us to assign the labeled features in Figure 4 as presented in Table 4.

The PGOPHER software package was used to simulate and fit rotational envelopes with rotational constants from the ic-MRCI-F12/cc-pVTZ-F12 optimized geometries (Table S5).[81] This package calculates the rotational stick spectrum (with $-2 \leq \Delta J \leq +2$) for a vibrational transition at a specified temperature and convolutes it with a Gaussian profile of a

DOI: 10.1021/jacs.6b10233
J. Am. Chem. Soc. 2016, 138, 16417−16425

Table 4. Assignments of Rotational Features for the Vibrational Origins of the $\tilde{b}$ and $\tilde{A}$ Bands in the SEVI Spectrum of Vinylidene

feature	anion		$K_{neutral} \leftarrow K_{anion}$
a	p-H_2CC^-	o-D_2CC^-	$0 \leftarrow 1$
b	o-H_2CC^-	p-D_2CC^-	$1 \leftarrow 0$
c	p-H_2CC^-	o-D_2CC^-	$2 \leftarrow 1$

specified width, which was used to obtain uncertainties in experimental peak positions. As the $\tilde{A}$ band shows more regularity in the spacing between and rotational contours of different vibrational features, the temperature, convolution width, and transition energy for the $\tilde{A}$ band origins were optimized simultaneously, giving ion temperatures of 13.4(1) and 14.2(2) K for H_2CC^- and D_2CC^-, respectively, indicating that virtually all anions are in rotational levels with $J < 10$. These temperatures are in good agreement with ion temperatures extracted in previous cryo-SEVI experiments.[74,79] These temperatures were used for fitting the $\tilde{b}$ band origins, for which only the transition energies and convolution widths were varied. For the rest of the assigned features, only the transition energy was optimized, providing precise extraction of vibrational frequencies. Minor variations in rotational profiles were observed across the different features in both electronic bands (see Figures S2 and S3), likely due to threshold effects on the detachment cross section as well as the apparent anharmonicity of these excited states revealed in the ν_2 progressions.

Non-Adiabaticity of Excited Vinylidene. We finally turn our attention to the eBE = 25 000−28 000 cm^{-1} region of the cryo-SEVI spectra, which consists of the $\tilde{b}$ electronic band as well as a number of anomalous features. As mentioned earlier, the intensities of the unassigned peaks relative to assigned vibrational features are not temperature dependent, which suggests that they solely reflect the vibronic structure of neutral, rather than anionic, vinylidene. The shifts of several of these peaks relative to the $\tilde{b}$ band origin (Table S6) are smaller than the smallest harmonic frequency expected for vinylidene, indicating that they cannot correspond to detachment to nominally forbidden vibrational levels in the $\tilde{b}$ $^3A_2$ state. Coupling to acetylene can in principle lead to perturbation of the photoelectron spectrum provided the barrier for isomerization to *trans*-HCCH is sufficiently low on the $\tilde{b}$ electronic surface, but the calculated barrier height of >2 eV indicates that isomerization is unlikely to play a role for the detachment energies considered here.

It is conceivable, however, that the anomalous peaks stem from mixing with vibrational levels in other electronic states, due, for example, to nonadiabatic coupling between the $\tilde{a}$ and $\tilde{b}$ triplet states or spin−orbit coupling between the $\tilde{A}$ state and the lower-lying triplet states. As the spin−orbit coupling is typically quite small for hydrocarbons, the latter option is unlikely to play a role in the electronic structure of H_2CC.

Figure 6 shows one-dimensional potential energy curves calculated for the adiabatic and diabatic $\tilde{a}$, $\tilde{b}$, and $\tilde{A}$ states along the carbon−carbon bond length (r_{CC}) coordinate, with all other coordinates fixed at the vinylidene $\tilde{b}$ state equilibrium geometry. A conical intersection between the $\tilde{a}$ and $\tilde{b}$ states is found ~0.05 eV above the $\tilde{b}$ state minimum; a two-dimensional depiction of the intersecting surfaces is shown in the bottom panel of Figure S1. The binding energies of the anomalous features in Figure 3 suggest detachment to neutral states that are in the energetic vicinity (within 0.2 eV) of the $\tilde{b}$

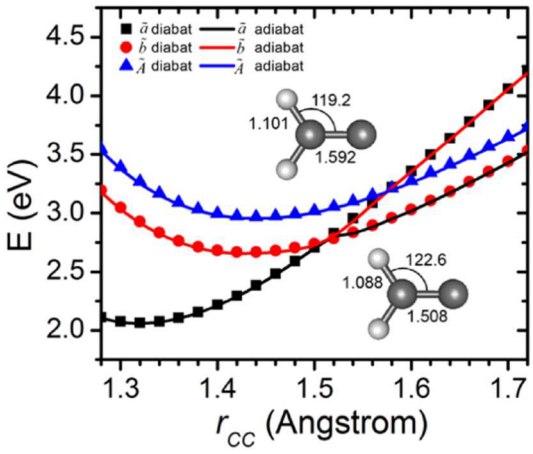

Figure 6. 1D potential energy curves of the adiabatic (lines) and diabatic (symbols) $\tilde{a}$ (black), $\tilde{b}$ (red), and $\tilde{A}$ (blue) states of vinylidene as functions of r_{CC}. Diabatic and adiabatic states are obtained from symmetry-controlled ab initio calculations and the PIP-NN-PESs, respectively. Energies are relative to the ground state of vinylidene, and structures of the two minimum crossing points obtained from the PESs are shown (bonds in Å, angles in degrees).

state minimum, so the $\tilde{a}$-$\tilde{b}$ crossing is a compelling candidate as an explanation for the observed structure.

At such an intersection of electronic states, vibrational levels taken to belong to separate electronic states are no longer independent, and can mix with each other. The resultant vibronic levels typically show features of both electronic states and are often responsible for dynamical processes such as internal conversion.[82,83] In an optical excitation, such mixing results in intensity borrowing by "dark" levels from "bright" states, resulting in transitions to nominally forbidden levels. An example is the ultraviolet absorption spectrum of SO_2 in the Clements band, in which the unassignable spectrum is attributed to the strong mixing between dipole forbidden and dipole allowed states, also induced by a conical intersection. Indeed, recent theoretical studies showed the Clements band structure is not well-described by an adiabatic model, but consideration of nonadiabatic coupling successfully accounts for the observed features.[84,85]

In vinylidene, within the adiabatic picture, the vibrational origin and a few low-lying levels of the $\tilde{b}$ state have good FC overlap with the anion ground state, and thus appear in the calculated spectra in Figure 3. High-lying vibrational levels of the $\tilde{a}$ state that lie near the $\tilde{b}$ state origin have poor FC overlap with the anion and hence do not appear in the calculated spectra. The observation of many more peaks in the experimental spectra than in the calculations suggests that that the low-lying, FC-active vibrational levels of the $\tilde{b}$ state are strongly mixed with high-lying vibrational levels of the $\tilde{a}$ state due to the conical intersection, leading to FC intensity-borrowing among these $\tilde{a}$ state levels. Although detachment to both the $\tilde{b}$ and $\tilde{a}$ states is allowed, their mixing via the conical intersection is likely to perturb the positions of the vibronic levels and alter the intensities. In the limit of linear vibronic coupling, the two states are coupled by the b_1 out-of-plane vibration; however, a thorough treatment of the derivative coupling and conical intersection requires careful diabatization to allow full-dimensional quantum characterization of mode-specific nonadiabatic dynamics. While currently feasible for

DOI: 10.1021/jacs.6b10233
J. Am. Chem. Soc. 2016, 138, 16417−16425

four-atom systems,[86] such a study is quite involved and beyond the scope of the current work.

In addition to the anomalous vibrational structure, the nonadiabaticity tied to the calculated intersection along the r_{CC} coordinate is reflected in the observed rotational contours of features assigned to the $\tilde{b}$ and $\tilde{A}$ electronic bands. As seen in Figures S2 and S3, the rotational profile shows more variation across the different vibrational features in the $\tilde{b}$ electronic band. This enhanced perturbation for the $\tilde{b}$ state rotational profiles is attributed to the $\tilde{a}$-$\tilde{b}$ conical intersection near the $\tilde{b}$ state minimum.

There is also an intersystem crossing between the diabatic $\tilde{a}$ and $\tilde{A}$ states ~0.25 eV above the $\tilde{A}$ state minimum. This crossing lies among the higher vibrational levels we see detachment to in the $\tilde{A}$ state, but given the agreement with theory for this electronic band, this crossing does not significantly impact the observed structure and thus is likely a weaker interaction than the $\tilde{a}$–$\tilde{b}$ conical intersection.

The low rotational temperatures extracted from the present spectra suggest interesting implications for the future application of the cryo-SEVI method to the $\tilde{X}\ ^1A_1 \leftarrow \tilde{X}\ ^2B_2$ electronic band of the vinylidene spectrum. Ervin and coworkers[16] estimated a rotational temperature of 150 K from the width of the $\tilde{a}$ band origin in their photoelectron spectra, and used this temperature to extract lifetime-broadening of <200 fs for the peaks in the $\tilde{X}$ band. This lifetime corresponds not to a relaxation into a continuum of states, but rather a quasi-continuum of acetylene states that were too dense to be resolved in their experiment. As pointed out by Fernando et al.,[21] rotational excitation can promote intramolecular vibrational relaxation (IVR) and increase the density of acetylene vibrational levels available for isomerization, in which case the lifetime for the isomerization of ground state vinylidene to HCCH can be strongly dependent on rotational temperature. Additionally, consideration of IVR of rovibrationally excited acetylene in its ground electronic state has shown that for the level of rotational excitation observed in the current work, the rate of IVR is significantly reduced, further decreasing the likelihood of lifetime-limited resolution.[87,88] Thus, application of the cryo-SEVI method to study the ground state band of vinylidene may reflect different dynamics than those observed in the previously reported photoelectron spectrum, and remains an ongoing effort in our laboratory.

CONCLUSIONS

Newly resolved vibronic structure in the excited state region of the vinylidene photoelectron spectrum is presented, yielding new insight into this model system and demonstrating that, in contrast to the ground state, electronically excited vinylidene is entirely decoupled from the acetylene isomer. The excited states of vinylidene prove to be spectroscopically interesting in their own right, and the reported spectra provide insight into possible spectroscopic manifestations of nonadiabatic effects in small molecules.

By photodetaching from cryogenically cooled vinylidene anions, well-resolved transitions to the $\tilde{a}\ ^3B_2$ and $\tilde{b}\ ^3A_2$ triplet states are seen, and the $\tilde{A}\ ^1A_2$ excited singlet state of H_2CC is observed experimentally for the first time. Highly accurate potential energy surfaces based on ab initio calculations of the acetylene–vinylidene system have been developed and quantum dynamical calculations on the resultant adiabatic potential energy surfaces have successfully reproduced part of the experimental spectrum, helping to assign the vibrational features. In addition, irregular vibrational features near the $\tilde{b}\ ^3A_2 \leftarrow \tilde{X}\ ^2B_2$ origin are found to be a manifestation of the conical intersection between the $\tilde{a}$ and $\tilde{b}$ electronic states in the vicinity of the vinylidene $\tilde{b}\ ^3A_2$ minimum. These features are attributed to a mixing of vibronic states that arises from nonadiabatic coupling, though definitive assignment of the transitions is not attempted in this work.

ASSOCIATED CONTENT

Supporting Information

The Supporting Information is available free of charge on the ACS Publications website at DOI: 10.1021/jacs.6b10233.

Detailed theoretical results, vinylidene rotational constants, rotational contours for all vibrational features in the $\tilde{b}$ and $\tilde{A}$ bands, and binding energies of the anomalous structure (PDF)

AUTHOR INFORMATION

Corresponding Authors

*bjiangch@ustc.edu.cn
*dneumark@berkeley.edu

ORCID

Jessalyn A. DeVine: 0000-0003-0091-4286
Marissa L. Weichman: 0000-0002-2551-9146
Xueyao Zhou: 0000-0002-7038-9360
Jianyi Ma: 0000-0001-8774-582X
Bin Jiang: 0000-0003-2696-5436
Hua Guo: 0000-0001-9901-053X
Daniel M. Neumark: 0000-0002-3762-9473

Notes

The authors declare no competing financial interest.

ACKNOWLEDGMENTS

This research is funded by the Air Force Office of Scientific Research (No. FA9550-16-1-0097 to D.M.N.), by the US Department of Energy (No. DE-SC0015997 to H.G.), and by the National Natural Science Foundation of China (No. 91441107 to J.M. and No. 21573203 to B.J.). M.L.W. thanks the National Science Foundation for a graduate research fellowship. The authors thank Robert Field for many useful discussions.

REFERENCES

(1) Skell, P. S.; Villaume, J. E.; Fagone, F. A. *J. Am. Chem. Soc.* **1972**, *94*, 7866–7867.
(2) Hatzikos, G. H.; Masel, R. I. *Surf. Sci.* **1987**, *185*, 479–494.
(3) Hills, M. M.; Parmeter, J. E.; Weinberg, W. H. *J. Am. Chem. Soc.* **1987**, *109*, 4224–4232.
(4) Ahmed, M.; Peterka, D. S.; Suits, A. G. *J. Chem. Phys.* **1999**, *110*, 4248–4253.
(5) Schaefer, H. F. *Acc. Chem. Res.* **1979**, *12*, 288–296.
(6) Carrington, T., Jr.; Hubbard, L. M.; Schaefer, H. F.; Miller, W. H. *J. Chem. Phys.* **1984**, *80*, 4347–4354.
(7) Duran, R. P.; Amorebieta, V. T.; Colussi, A. J. *J. Am. Chem. Soc.* **1987**, *109*, 3154–3155.
(8) Schork, R.; Koppel, H. *Theor. Chem. Acc.* **1998**, *100*, 204–211.
(9) Hayes, R. L.; Fattal, E.; Govind, N.; Carter, E. A. *J. Am. Chem. Soc.* **2001**, *123*, 641–657.
(10) Schork, R.; Koppel, H. *J. Chem. Phys.* **2001**, *115*, 7907–7923.
(11) Zou, S.; Bowman, J. M.; Brown, A. *J. Chem. Phys.* **2003**, *118*, 10012–10023.
(12) Joseph, S.; Varandas, A. J. C. *J. Phys. Chem. A* **2010**, *114*, 13277–13287.

(13) Ren, Y.; Li, B.; Bian, W. *Phys. Chem. Chem. Phys.* **2011**, *13*, 2052−2061.
(14) Han, H.; Li, A.; Guo, H. *J. Chem. Phys.* **2014**, *141*, 244312.
(15) Lundberg, J. K.; Field, R. W.; Sherrill, C. D.; Seidl, E. T.; Xie, Y.; Schaefer, H. F. *J. Chem. Phys.* **1993**, *98*, 8384−8391.
(16) Ervin, K. M.; Ho, J.; Lineberger, W. C. *J. Chem. Phys.* **1989**, *91*, 5974−5992.
(17) Stanton, J. F.; Gauss, J. *J. Chem. Phys.* **1999**, *110*, 6079−6080.
(18) Laufer, A. H. *J. Chem. Phys.* **1980**, *73*, 49−52.
(19) Laufer, A. H. *J. Chem. Phys.* **1982**, *76*, 945−948.
(20) Chen, C.; Braams, B.; Lee, D. Y.; Bowman, J. M.; Houston, P. L.; Stranges, D. *J. Phys. Chem. Lett.* **2010**, *1*, 1875−1880.
(21) Fernando, R.; Qu, C.; Bowman, J. M.; Field, R. W.; Suits, A. G. *J. Phys. Chem. Lett.* **2015**, *6*, 2457−2462.
(22) Jacobson, M. P.; Field, R. W. *J. Phys. Chem. A* **2000**, *104*, 3073−3086.
(23) Thissen, R.; Delwiche, J.; Robbe, J. M.; Duflot, D.; Flament, J. P.; Eland, J. H. D. *J. Chem. Phys.* **1993**, *99*, 6590−6599.
(24) Osipov, T.; Cocke, C. L.; Prior, M. H.; Landers, A.; Weber, T.; Jagutzki, O.; Schmidt, L.; Schmidt-Bocking, H.; Dorner, R. *Phys. Rev. Lett.* **2003**, *90*, 233002.
(25) King, G. W.; Ingold, C. K. *Nature* **1952**, *169*, 1101−1102.
(26) Ingold, C. K.; King, G. W. *J. Chem. Soc.* **1953**, *0*, 2702−2704.
(27) Ingold, C. K.; King, G. W. *J. Chem. Soc.* **1953**, 2704−2707.
(28) Lassettre, E. N.; Skerbele, A.; Dillon, M. A. *J. Chem. Phys.* **1968**, *49*, 2382.
(29) Burton, C. S.; Hunziker, H. E. *J. Chem. Phys.* **1972**, *57*, 339.
(30) Wendt, H. R.; Hippler, H.; Hunziker, H. E. *J. Chem. Phys.* **1979**, *70*, 4044−4048.
(31) Watson, J. K. G.; Herman, M.; Craen, J. C. V.; Colin, R. *J. Mol. Spectrosc.* **1982**, *95*, 101−132.
(32) Burnett, S. M.; Stevens, A. E.; Feigerle, C. S.; Lineberger, W. C. *Chem. Phys. Lett.* **1983**, *100*, 124.
(33) Sulzle, D.; Schwarz, H. *Chem. Phys. Lett.* **1989**, *156*, 397−400.
(34) Levin, J.; Feldman, H.; Baer, A.; Ben-Hamu, D.; Heber, O.; Zajfman, D.; Vager, Z. *Phys. Rev. Lett.* **1998**, *81*, 3347−3350.
(35) Gerardi, H. K.; Breen, K. J.; Guasco, T. L.; Weddle, G. H.; Gardenier, G. H.; Laaser, J. E.; Johnson, M. A. *J. Phys. Chem. A* **2010**, *114*, 1592−1601.
(36) Conrad, M. P.; Schaefer, H. F. *J. Am. Chem. Soc.* **1978**, *100*, 7820−7823.
(37) Dykstra, C. E.; Schaefer, H. F. *J. Am. Chem. Soc.* **1978**, *100*, 1378−1382.
(38) Vacek, G.; Thomas, J. R.; DeLeeuw, B. J.; Yamaguchi, Y.; Schaefer, H. F. *J. Chem. Phys.* **1993**, *98*, 4766−4776.
(39) Stanton, J. F.; Huang, C. M.; Szalay, P. G. *J. Chem. Phys.* **1994**, *101*, 356−365.
(40) Stanton, J. F.; Gauss, J. *J. Chem. Phys.* **1994**, *101*, 3001−3005.
(41) Sherrill, C. D.; Byrd, E. F. C.; Head-Gordon, M. *J. Chem. Phys.* **2000**, *113*, 1447−1454.
(42) Boyé-Péronne, S.; Gauyacq, D.; Liévin, J. *J. Chem. Phys.* **2014**, *141*, 174317.
(43) Guo, L.; Han, H.; Ma, J.; Guo, H. *J. Phys. Chem. A* **2015**, *119*, 8488−8496.
(44) Neumark, D. M. *J. Phys. Chem. A* **2008**, *112*, 13287−13301.
(45) Gibson, S. *Laser Physics Centre*; Australian National University: Canberra, Australia, Personal communication, 2016.
(46) Osterwalder, A.; Nee, M. J.; Zhou, J.; Neumark, D. M. *J. Chem. Phys.* **2004**, *121*, 6317−6322.
(47) Weichman, M. L.; DeVine, J. A.; Levine, D. S.; Kim, J. B.; Neumark, D. M. *Proc. Natl. Acad. Sci. U. S. A.* **2016**, *113*, 1698−1705.
(48) Even, U.; Jortner, J.; Noy, D.; Lavie, N.; Cossart-Magos, C. *J. Chem. Phys.* **2000**, *112*, 8068−8071.
(49) Dawson, J. H. J.; Jennings, K. R. *J. Chem. Soc., Faraday Trans. 2* **1976**, *72*, 700−706.
(50) Hock, C.; Kim, J. B.; Weichman, M. L.; Yacovitch, T. I.; Neumark, D. M. *J. Chem. Phys.* **2012**, *137*, 224201.
(51) Wiley, W. C.; Mclaren, I. H. *Rev. Sci. Instrum.* **1955**, *26*, 1150−1157.
(52) Eppink, A. T. J. B.; Parker, D. H. *Rev. Sci. Instrum.* **1997**, *68*, 3477−3484.
(53) Chandler, D. W.; Houston, P. L. *J. Chem. Phys.* **1987**, *87*, 1445−1447.
(54) Doyle, M. B.; Abeyasera, C.; Suits, A. G.*NuACQ*, http://chem.wayne.edu/suitsgroup/NuAcq.html (accessed December 3, 2016).
(55) Dick, B. *Phys. Chem. Chem. Phys.* **2014**, *16*, 570.
(56) Blondel, C.; Delsart, C.; Goldfarb, F. *J. Phys. B: At., Mol. Opt. Phys.* **2001**, *34*, L281−L288.
(57) Shiozaki, T.; Knizia, G.; Werner, H. J. *J. Chem. Phys.* **2011**, *134*, 034113.
(58) Knowles, P. J.; Werner, H.-J. *Chem. Phys. Lett.* **1985**, *115*, 259−267.
(59) Werner, H.-J.; Knowles, P. J. *J. Chem. Phys.* **1985**, *82*, 5053−5063.
(60) Peterson, K. A.; Adler, T. B.; Werner, H.-J. *J. Chem. Phys.* **2008**, *128*, 084102.
(61) Werner, H. J.; Knowles, P. J.; Knizia, G.; Manby, F. R.; Schütz, M. *WIREs Comput. Mol. Sci.* **2012**, *2*, 242−253.
(62) Jiang, B.; Guo, H. *J. Chem. Phys.* **2013**, *139*, 054112−5.
(63) Li, J.; Jiang, B.; Guo, H. *J. Chem. Phys.* **2013**, *139*, 204103−7.
(64) Jiang, B.; Li, J.; Guo, H. *Int. Rev. Phys. Chem.* **2016**, *35*, 479.
(65) Xie, Z.; Bowman, J. M. *J. Chem. Theory Comput.* **2010**, *6*, 26−34.
(66) Braams, B. J.; Bowman, J. M. *Int. Rev. Phys. Chem.* **2009**, *28*, 577−606.
(67) Yu, H.-G.; Muckerman, J. T. *J. Mol. Spectrosc.* **2002**, *214*, 11−20.
(68) Chen, R.; Ma, G.; Guo, H. *J. Chem. Phys.* **2001**, *114*, 4763−4774.
(69) Echave, J.; Clary, D. C. *Chem. Phys. Lett.* **1992**, *190*, 225−230.
(70) Wei, H.; Carrington, T., Jr. *J. Chem. Phys.* **1992**, *97*, 3029−3037.
(71) Guo, H. *Rev. Comput. Chem.* **2007**, *25*, 285−347.
(72) Chen, R.; Guo, H. *Comput. Phys. Commun.* **1999**, *119*, 19−31.
(73) Guo, H. *J. Chem. Phys.* **1998**, *108*, 2466−2472.
(74) Kim, J. B.; Hock, C.; Yacovitch, T. I.; Neumark, D. M. *J. Phys. Chem. A* **2013**, *117*, 8126−8131.
(75) Cooper, J.; Zare, R. N. *J. Chem. Phys.* **1968**, *48*, 942.
(76) Wigner, E. P. *Phys. Rev.* **1948**, *73*, 1002−1009.
(77) Herzberg, G. *Infrared and Raman Spectra of Polyatomic Molecules*; D. Van Nostrand Company, Inc.: Princeton, NJ, 1945; Vol. *2*.
(78) Lee, H.; Baraban, J. H.; Field, R. W.; Stanton, J. F. *J. Phys. Chem. A* **2013**, *117*, 11679−11683.
(79) Weichman, M. L.; Kim, J. B.; Neumark, D. M. *J. Chem. Phys.* **2014**, *140*, 104305.
(80) Bunker, P. R.; Jensen, P. *Molecular Symmetry and Spectroscopy*, 2nd ed.; NRC Research Press: Ottawa, 2006.
(81) Western, C. M. *PGOPHER, a program for simulating rotational structure* **2010**.
(82) Bixon, M.; Jortner, J. *J. Chem. Phys.* **1968**, *48*, 715.
(83) Schneider, R.; Domcke, W. *Chem. Phys. Lett.* **1988**, *150*, 235.
(84) Xie, C.; Hu, X.; Zhou, L.; Xie, D.; Guo, H. *J. Chem. Phys.* **2013**, *139*, 014305.
(85) Leveque, C.; Komainda, A.; Taieb, R.; Koppel, H. *J. Chem. Phys.* **2013**, *138*, 044320.
(86) Guo, H.; Yarkony, D. R. *Phys. Chem. Chem. Phys.* **2016**, *18*, 26335−26352.
(87) Perry, D. S.; Miller, A.; Amyay, B.; Fayt, A.; Herman, M. *Mol. Phys.* **2010**, *108*, 1115−1132.
(88) Perry, D. S.; Martens, J.; Amyay, B.; Herman, M. *Mol. Phys.* **2012**, *110*, 2687−2705.

DOI: 10.1021/jacs.6b10233
J. Am. Chem. Soc. 2016, 138, 16417−16425